Optoelectrostatic storage ring for polar molecules from supersonic expansion

Zhenghai Yang,[1] Lianzhong Deng,[1,*] Bin Wei,[1] Shaojie Wang,[2] Shunyong Hou,[1] and Jianping Yin[1]
[1]*State Key Laboratory of Precision Spectroscopy, School of Physics and Material, East China Normal University, Shanghai 200062, China*
[2]*College of Electrical and Information Engineering, Shaoyang University, Shaoyang 422000, China*

(Received 25 January 2019; published 18 March 2019)

Cold molecules are desired in a wide range of research areas, like precision measurement of physical constants, high-resolution spectroscopy, and cold collisions. Scientific interest in the generation and manipulation of cold molecules has been strong for decades. Here we theoretically investigate the dynamics of an optoelectrostatic storage ring for polar molecules, which is composed of an orbiting laser beam and an electrostatic quadrupole ring. The potentials of water molecules experienced in the combined optical and electrical fields are first calculated and a three-dimensional (3D) hybrid potential well for molecules of interest is formed in the focus spot of the red-detuned laser beam. The behavior of motional water molecules under the influence of the decelerating hybrid potential well is then investigated. Later, the deceleration and trapping processes of water molecules from supersonic expansion in the hybrid potential well are numerically simulated and corresponding results are presented. Our study indicates that this optoelectrostatic storage ring, featuring a 3D potential well of controllable orbiting speed, can serve as a good platform for production and manipulation of cold polar molecules and should have important applications in the related research areas.

DOI: 10.1103/PhysRevA.99.033414

I. INTRODUCTION

Cold and ultracold molecules have long been a good platform for new insights into many disciplines, such as precision measurements [1], cold collision and cold chemistry [2], novel many-body quantum systems [3], interferometers [4], and quantum information processing [5]. So far, various methods have been proposed and demonstrated for the production of cold or ultracold molecules, including association of ultracold atoms [6,7], laser cooling [8,9], electrostatic Stark deceleration [10], Zeeman deceleration [11], optical Stark deceleration [12–14], collisional deceleration [15], photon dissociation [16], buffer gas cooling [17], optoelectrical cooling [18], and so on. Each method has its own advantages and disadvantages, and efforts in pursuit of new principles and schemes for production of cold molecules have never ceased.

When the molecules are slow enough they can be either trapped locally [19] or confined in a storage ring. The idea of confining polar molecules inside an electrostatic storage ring was first proposed by Katz [20] and later demonstrated in experiment by Crompvoets *et al.* [21]. The cold molecular packet confined in the storage ring can repeatedly appear at selected positions or eject tangentially out of the ring at a selected point under control, and is thus suitable for studies like low-energy collisions, cold chemical reactions, and precision measurements. Since then a number of experimental and theoretical studies on storage rings for cold polar molecules have been reported [22–25]. Up to now, all the molecular packets loading the storage ring were from the electrostatic Stark decelerator. The electrostatic Stark decelerator depends on precise time control of the interaction between the molecular electric dipole moment (EDM) and the electrical fields to remove the kinetic energy of the fast-moving polar molecules from supersonic expansion. It usually works well in decelerating light linear and symmetric top molecules with a large ratio of EDM to mass, like CO, CH, OH, NH_3/ND_3, and CH_3F, but has difficulty in decelerating most asymmetric top molecules, even small ones like H_2O [26]. Fortunately, some of those molecules have a relatively large ratio of polarizability to mass and thus can be efficiently decelerated using a strong laser field. A spatially localized laser focus works much like a single-stage optical Stark decelerator and has demonstrated in experiment its capacity in slowing fast-moving molecules, though precise control on the molecule velocity has not achieved [13]. A moving laser focus can, however, provide long time interaction between the laser field and molecules, and bring better control on the velocity of the decelerated molecules. Deceleration of supersonic molecular beams using a rotating laser beam was first proposed by Friedrich [12] and later theoretically investigated by our group [27,28]. However, the orbiting focus spot of the red-detuned laser beam creates only a two-dimensional (2D) optical potential well, and the confinement of the molecules in the laser propagation direction is negligibly weak. This means that the molecules keep expanding in the laser propagation direction during the process of deceleration. The molecules will finally get lost when they expand out of the laser focus spot.

In this paper, we propose and investigate a hybrid optoelectrostatic storage ring, consisting of a rotating laser beam and an electrostatic quadrupole ring. Polar molecules from supersonic expansion can be first decelerated to any desired speed and then trapped inside the hybrid storage ring. The water molecule $H_2{}^{16}O$ is taken as an example to test the performance of our scheme. The potential experienced by the H_2O molecule inside the combined optical and electrical

*lzdeng@phy.ecnu.edu.cn

fields is first calculated. Then, the dynamic behavior of the H_2O molecule inside the decelerating hybrid potential well is theoretically investigated. Later, the deceleration and trapping processes of H_2O molecular beams from supersonic expansion are numerically simulated using the Monte Carlo method. The spatial and velocity distributions of the decelerated molecular packet are analyzed. Some discussion and a brief summary are given in the end.

Water is fundamental to life and human activities, and is one of the most abundant resources on Earth. As the most important molecule, water is widely involved in various kinds of physical and chemical processes. Water has also been detected in interstellar clouds [29], where the temperature and density might be rather low. Studies on interactions of slow (cold) water molecules with other particles can help us not only in further understanding their physical and chemical properties but also in getting knowledge on how to capture and collect gaseous water for human use in future outer space traveling. Due to its asymmetric top structure, the H_2O molecule is difficult to be decelerated using the conventional electrostatic Stark decelerator [26]. Fortunately, due to its large ratio of polarizability ($\alpha = 1.6 \times 10^{-40}\,\mathrm{C\,m^2\,V^{-1}}$) to mass this molecule can be efficiently decelerated using a laser field.

II. SCHEME AND DECELERATION PRINCIPLE

A. Scheme

Figure 1 shows the schematic diagram of our proposed optoelectrostatic storage ring for decelerating and trapping polar molecules from supersonic expansion. A focusing laser beam propagates from the top down and gets reflected horizontally via a spinning reflective mirror. An orbiting laser focus spot is obtained in the horizontal plane and serves as a traveling 2D optical potential well for molecules when the laser is red detuned. The electrostatic quadrupole ring offers additional confinement for weak-field-seeking molecules in the laser propagation direction. Thus, an orbiting three-dimensional (3D) optoelectrical potential well for polar molecules is formed in the laser focus spot. Polar molecules from supersonic expansion enter the storage ring tangentially and are captured by the traveling 3D potential well. By reducing the spinning speed of the reflective mirror, the orbiting 3D potential well will be decelerated, and so will the molecules captured inside. For convenience of description and analysis, two frames of reference are introduced and shown in Fig. 1. One is fixed in the lab and indicated by *XYZ*, the other is fixed on the moving laser focus (i.e., the potential well) center and indicated by *xyz*. The axes of Y and y are in the same direction. The angle between the laser propagation direction and the lab-fixed Z direction is denoted as θ.

B. Potential energy and dipole force

H_2O is a typical representative of asymmetric top molecules with its three rotational constants being $A = 27.861\,\mathrm{cm^{-1}}$, $B = 14.512\,\mathrm{cm^{-1}}$, and $C = 9.271\,\mathrm{cm^{-1}}$, respectively [30]. For an asymmetric top molecule, the term symbol of $|J, \tau, M\rangle$ is conventionally used to specify the quantum state. Figure 2 shows the Stark energy shifts of H_2O as a function of the electrical field magnitude for quantum states of $J = 1$ and $\tau = -1,\ 0,\ 1$, respectively. The results are obtained using the so-called matrix method [31], which is suitable for calculating energy shifts of molecules at external fields of arbitrary intensity. The weak-field-seeking state of $|J = 1, \tau = 1,\ |M| = 1\rangle$, marked by the hollow circle in Fig. 2, is conventionally thought to be a good option for electrostatic deceleration and trapping. For instance, the energy shift at an electrical field of 200 kV/cm is calculated to be about $0.45\,\mathrm{cm^{-1}}$ for this state.

The optical potential experienced by a molecule inside the red-detuned laser field can be expressed as [27]

$$U = -\frac{\alpha |E(r)|^2}{2} = -\left(\frac{\alpha}{C\varepsilon_0}\right) I(r)$$
$$= -\left(\frac{\alpha}{C\varepsilon_0}\right) I_0 \exp\left[-2\left(\frac{r}{\omega}\right)^2\right]. \quad (1)$$

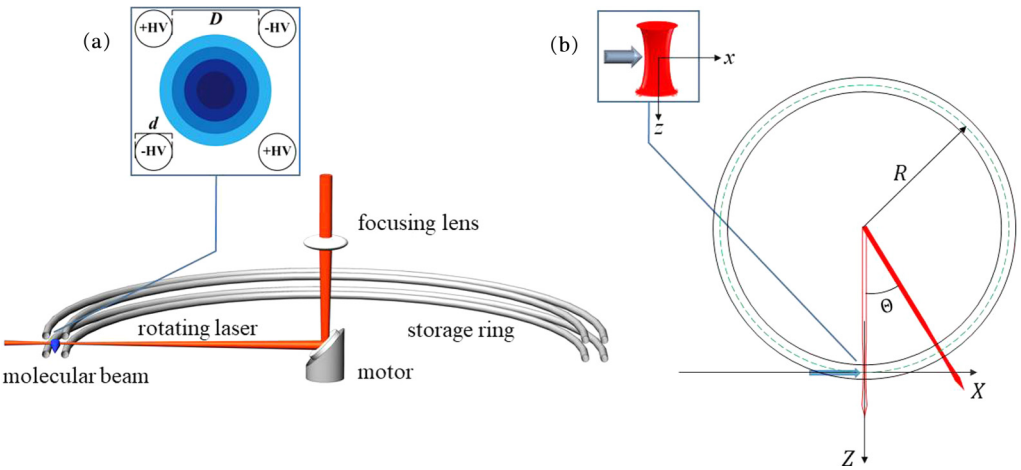

FIG. 1. Schematic diagram of the optoelectrostatic storage ring for polar molecules from supersonic expansion with (a) side view and (b) bird's-eye view. R is the radius of the electrostatic quadrupole ring. The inset in (a) shows a contour plot of the electrical field of the quadrupole trap and that in (b) indicates a close view of the laser focus spot.

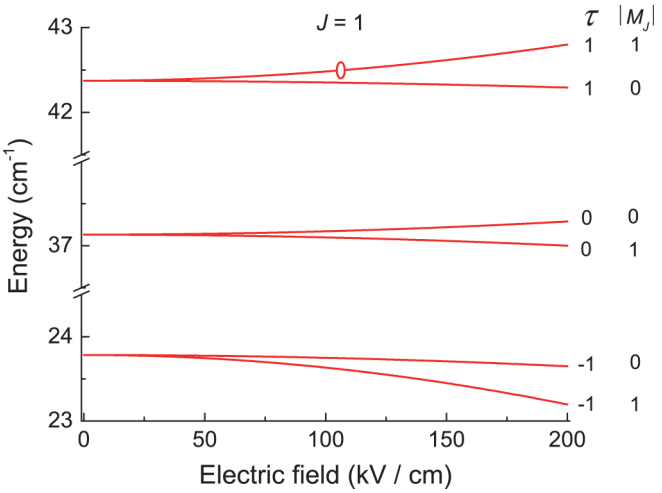

FIG. 2. The rotational energies of H_2O $|J, \tau, M\rangle$ states as a function of the electrical field strength ($J = 1$ and $\tau = -1,\ 0,\ 1$, respectively).

Here, α is the averaged polarizability of the molecule. The light field is assumed to have a Gaussian intensity distribution in the radial direction, i.e., $I(r) = I_0 \exp[-2(r/\omega)^2]$. Here r is the distance of the molecule from the laser beam axis. I_0 is the maximum laser intensity at $r = 0$ and is related to the laser power of P via the formula of $I_0 = 2P/\pi\omega^2$, and ω is the waist radius of the laser focus spot. $E(r)$ is the amplitude of the electrical field component and is related to the laser intensity $I(r)$ via the formula $I = \varepsilon_0 E^2 C/2$ with ε_0 the free space permittivity and C the speed of light in vacuum.

The total potential energy U_T experienced by the H_2O molecule of state $|J = 1, \tau = 1,\ |M| = 1\rangle$ exposed to the combined optical and electrical fields is numerically calculated using the above-mentioned matrix method. For our calculation here, a continuous-wave (CW) red-detuned laser of 40 kW is focused into a spot of diameter $2\omega = 80\,\mu$m with the peak laser intensity I_0 being about $1.6 \times 10^9\,\mathrm{W/cm^2}$.

The quadrupole ring has a curvature radius of $R = 25$ cm and consists of four stainless steel electrode rods of diameter $d = 1$ mm. The surface-to-surface distance of the neighboring electrodes is $D = 1.5$ mm. The voltages applied on the neighboring electrodes are $+HV = 20$ kV and $-HV = -20$ kV, respectively. A hybrid 3D potential well is formed in the laser focus spot for molecules of interest. Figure 3 shows the spatial distribution of the 3D potential well for the H_2O molecule along the three axes of the reference frame of xyz fixed on the laser focus spot. As one can see, in the x and y directions the shape of the potential well is basically determined by the optical field and its scale is comparable to the waist spot size, as shown in Figs. 3(a) and 3(b). In the z direction the shape of the potential well is basically determined by the electrical field and its scale is comparable to the size of the quadrupole trap. The dipole force per unit mass experienced by the moving molecule inside the potential well can be obtained from the differential equation of $P(i) = F(i)/m = -\nabla U_T(i)/m$; here $i = x, y,$ or z. Figure 4 shows the corresponding values of $P(i)$ in the three directions of x, y, and z. As illustrated, the dipole force per unit mass experienced by the H_2O molecule is on the order of $10^5\,\mathrm{m/s^2}$ along the three directions of x, y, and z inside the potential well, but the confinement of molecules in the x and y directions is much stronger than that in the z direction. The maximal value of $P_m = \sim 9.73 \times 10^5\,\mathrm{m/s^2}$ is obtained in the x and y directions.

C. Longitudinal motion

During deceleration, the spinning mirror is under brake with an angular deceleration rate of γ, and the traveling potential well gets a linear deceleration rate of $a = R\gamma$ in the longitudinal (i.e., x) direction. The motion of a molecule relative to the hybrid potential well in the longitudinal direction is given by

$$m\frac{d^2x}{dt^2} + ma - F(x) = 0. \tag{2}$$

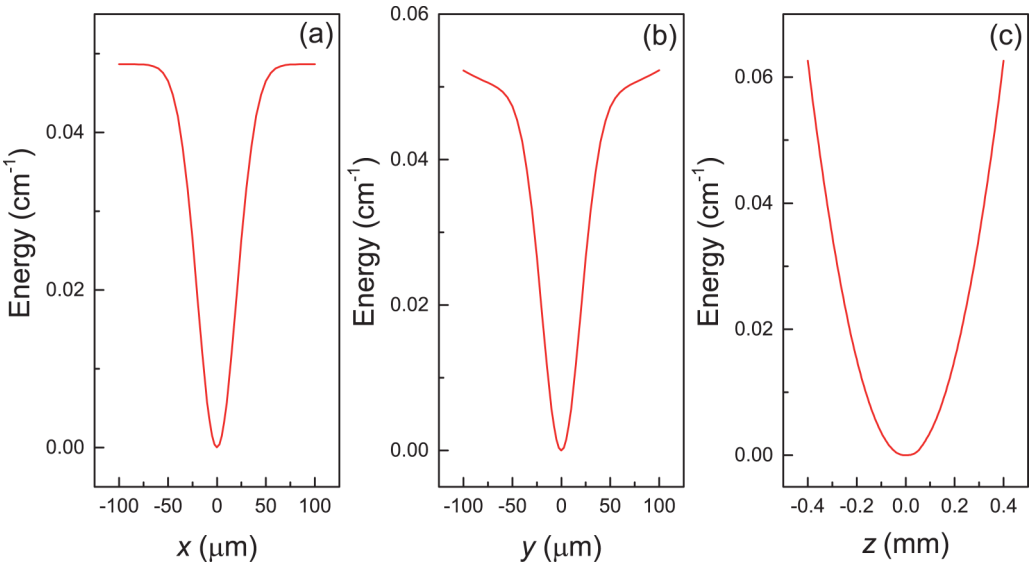

FIG. 3. The total potential energy U_T for the H_2O molecule of state $|J = 1, \tau = 1,\ |M| = 1\rangle$ along the three axes of the reference frame xyz.

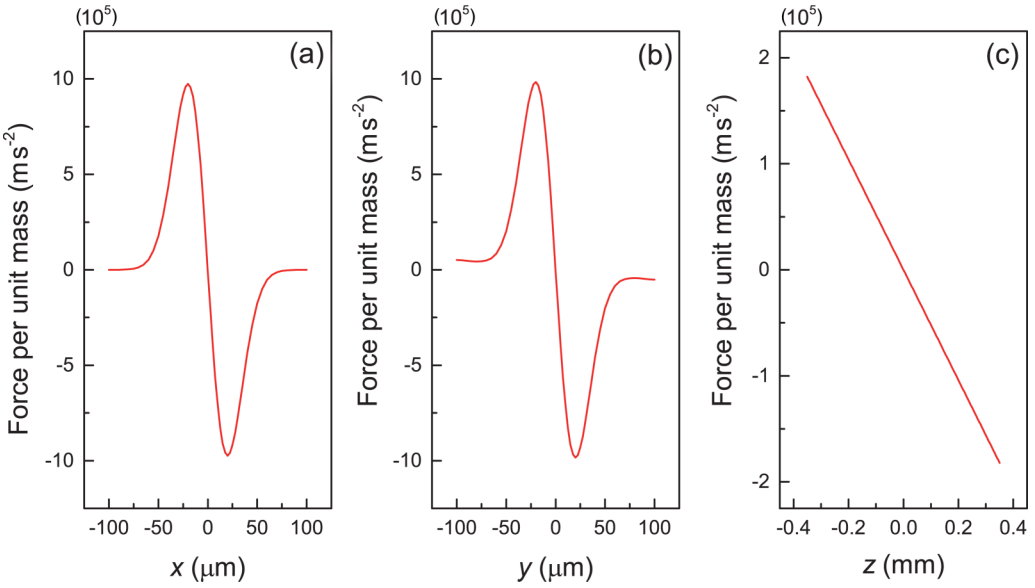

FIG. 4. The dipole force per unit mass, $P(i) = F(i)/m$, experienced by the H_2O molecule of state $|J = 1, \tau = 1, |M| = 1\rangle$ along the three axes of the reference frame xyz.

Here m is the mass of the molecule, x is the position difference between the molecule and the potential center, a is the deceleration rate of the potential well, and $F(x)$ is the force experienced by the molecule in the x direction. Let us introduce the relative velocity of the molecule with respect to the potential center, $v_x = dx/dt$. After transforming Eq. (2) and doing integration on both sides, one can get the following equation of motion for the molecule,

$$v_x^2 = 2\int\left[\frac{F(x)}{m} - a\right]dx + C_{\text{intg}} = 2\int [P(x) - a]dx + C_{\text{intg}}, \tag{3}$$

with C_{intg} being the integration constant. When the deceleration rate a is less than the maximal value of the dipole force per unit mass $P_m(x)$, there exists a stable area in the phase space, so-called phase acceptance. Based on the values of $P(x)$ as presented in Fig. 4, the phase stable area can be numerically determined by using Eq. (3) and solving the differential equation of $d(v_x^2)/dx = 0$. Molecules first captured in this area will follow the motion of the potential well and be decelerated accordingly, and molecules first outside this area might have their velocity somewhat influenced but cannot be stably decelerated along with the potential well. Figure 5(a) shows the trajectories of both trapped (solid lines) and untrapped (dashed lines) H_2O molecules in the phase space with $a = P_m/2 = 4.87 \times 10^5\ \text{m/s}^2$. Figure 5(b) shows the separatrices of the phase acceptance with the deceleration rate of $a = 0.25P_m$, $0.50P_m$, and $0.75P_m$, respectively; Fig. 5(c) shows the effective potential wells for H_2O molecules accordingly for the above selected values of a in this direction.

D. Transverse motion

The molecule with longitudinal velocity of v_x experiences a centrifugal force in the z direction when orbiting inside the storage ring in the xz plane. A pseudopotential energy contributed by the centrifugal force can be introduced and given as

$$U_{\text{centri}} = \int \text{F}_{\text{centri}} dz = -mv^2 \ln\left(1 + \frac{z}{R}\right), \tag{4}$$

where z is the transverse position away from the potential center and R is the curvature radius of the storage ring. The effective potential energy U_{eff} for molecules in the ring is the sum of the pseudopotential energy and the hybrid potential

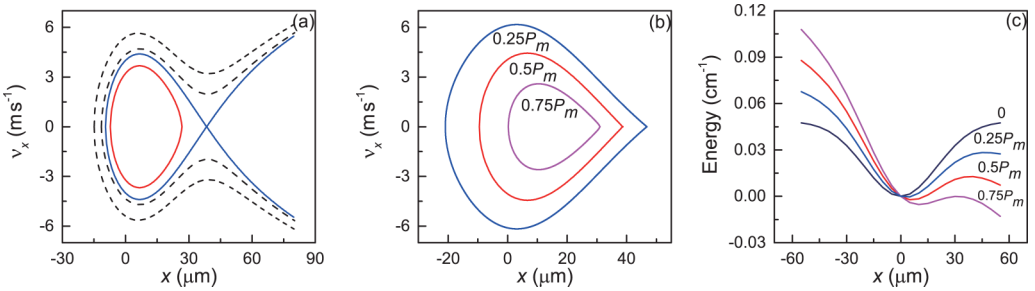

FIG. 5. (a) Trajectories of both trapped (solid lines) and untrapped (dashed lines) H_2O molecules in the phase space with $a = P_m/2 = 4.87 \times 10^5\ \text{m/s}^2$. (b) The separatrices of the phase acceptance for H_2O molecules with different deceleration rates of $a = 0.25P_m$, $0.50P_m$, and $0.75P_m$. (c) The effective potential wells for H_2O molecules with the selected values of a.

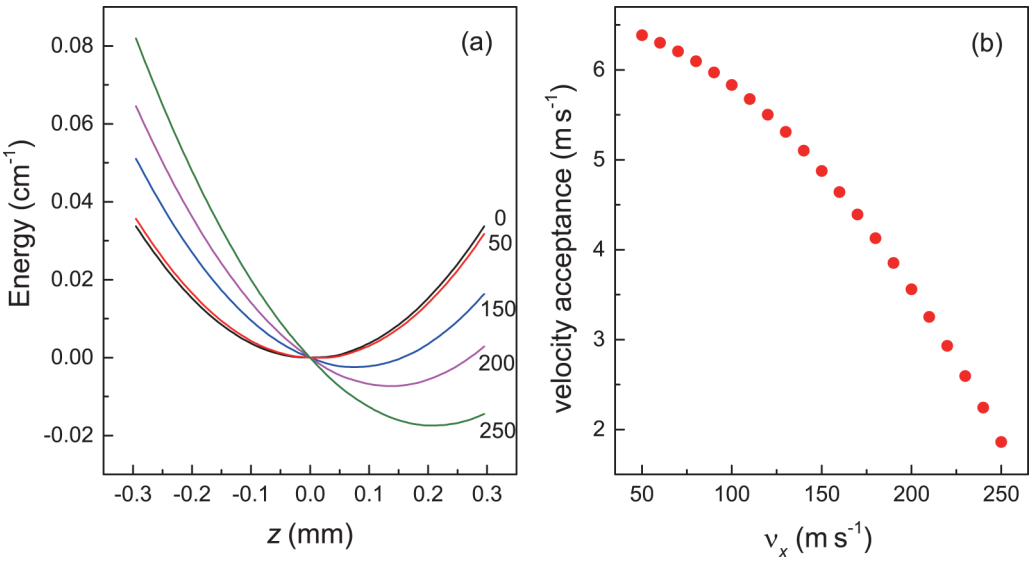

FIG. 6. (a) The effective potential well for the H_2O molecule for selected longitudinal velocities of $v_x = 0$, 50, 150, 200, and 250 m/s, respectively. (b) Velocity acceptance of the potential well in the direction of z as a function of the longitudinal velocity v_x.

energy U_z in the z direction.

$$U_{\text{eff}} = U_z - mv_x^2 \ln\left(1 + \frac{z}{R}\right). \tag{5}$$

Figure 6(a) shows the effective potential wells for the H_2O molecule for selected longitudinal velocities of $v_x = 0$, 50, 150, 200, and 250 m/s, respectively. With the increase of the longitudinal velocity v_x, the effective potential well for the molecules becomes shallow in depth with its center moving toward the positive z axis, as can be seen in Fig. 6(a). The confinement of molecules is mainly provided by the electrical field in the z direction. As discussed above, the potential well is deeper in depth and bigger in size in the z direction than in the two other directions of x and y. However, due to the coupling of the molecular motion in the longitudinal and transverse direction, the velocity acceptance of the molecules in the z direction is finally determined by the potential depth in the x direction, as will be confirmed in the following numeric simulation. Figure 6(b) shows the corresponding velocity acceptance of the potential well in the transverse direction of z as a function of the longitudinal velocity of v_x.

The molecules oscillate in the potential well when confined in the storage ring. The oscillation frequency of the confined molecules in the transverse direction can be approximately estimated from the expression of $f = \frac{1}{2\pi}\sqrt{-dp(i)/di}$ with $i = y$ or z. With the parameters used in Fig. 4, the oscillation frequency of the confined molecules are calculated to be about $\sim 4.3 \times 10^4$ Hz and $\sim 3.6 \times 10^3$ Hz in the y and z directions, respectively.

III. NUMERIC SIMULATIONS

In fact, due to the coupling of motion in the 3D space, the behavior of the molecule is rather complicated in the hybrid potential well. To better understand the dynamics of the molecules inside the optoelectrostatic storage ring, the deceleration and trapping processes of the H_2O molecular beam in the orbiting hybrid potential well are numerically simulated using the Monte Carlo method. The pulsed H_2O molecular beam from supersonic expansion is assumed to have a Gaussian velocity distribution centered at 250 m/s in the X direction with a translational temperature of 2 K in the laboratory frame. The transverse velocity is centered at zero with a full width at half maximum (FWHM) velocity spread of about 10 m/s. The parameters of the optoelectrostatic storage ring are the same as those mentioned in the above description. For loading molecules into the hybrid potential well, the laser focus spot intersects the central portion of the molecular beam with an orbiting speed of 250 m/s as well. The deceleration process starts at the position of $\theta = 0$ (i.e., $X = Y = Z = 0$ in the lab frame) and is operated by braking the spinning reflective mirror to reduce the orbiting speed of the laser focus spot. With a linear deceleration rate of $a = -P_m/2 = -4.87 \times 10^5$ m/s^2, the potential well can be decelerated from 250 to 50 m/s within a time interval of $\sim$411 μs. The orbiting laser focus spot covers an angle of $\theta = \sim 14.12^\circ$ with its new position in the lab frame being $X = R[\sin(\theta)] = 61.0$ mm, $Y = 0$, and $Z = -R[1 - \cos(\theta)] = -7.56$ mm. Red solid symbols in Fig. 7 show the spatial profile of the decelerated molecular packet in the XZ plane of the laboratory frame when the laser focus spot is decelerated to the speed of 200 ($\theta = \sim 5.30^\circ$), 150 ($\theta = \sim 9.42^\circ$), 100 ($\theta = \sim 12.36^\circ$), and 50 m/s ($\theta = \sim 14.12^\circ$), respectively. As illustrated in the figure, the decelerated molecular packet is well confined by the 3D hybrid potential trap and follows its orbiting trajectory in the storage ring. For comparison, the deceleration of the molecular beam with the laser field only (no electric field) is also simulated. The spatial profile of the molecular packet decelerated along with the laser focus spot is shown in Fig. 7 with blue solid symbols. With the absence of the electrical field, the orbiting laser focus spot serves only as a 2D trap for the decelerated molecules. Due to lack of confinement the decelerated molecular packet gradually expands along the laser propagation direction (i.e., the z direction fixed on the orbiting laser focus spot). The molecules finally get lost when they expand out of the laser focus spot, as shown by the black

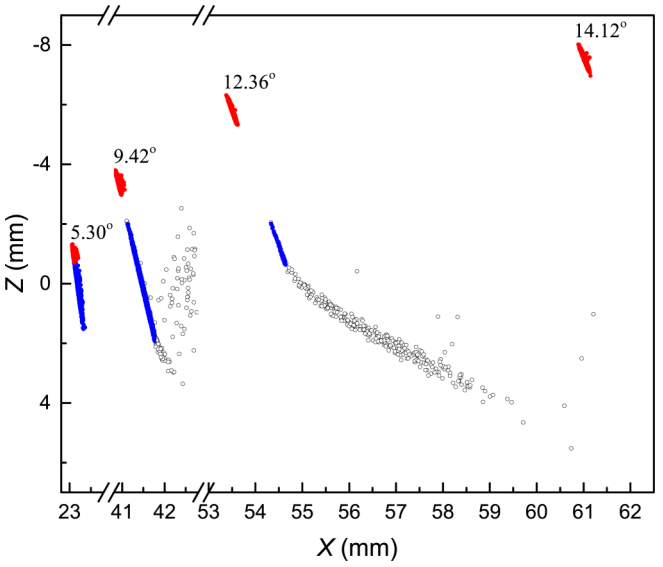

FIG. 7. The spatial distribution of the decelerated molecular packet in the plane of XZ of the laboratory frame for the cases of 3D hybrid potential well with combined laser-electrical fields (red solid symbols) and 2D potential well with laser field only (blue solid symbols). The black hollow symbols represent molecules which are first accepted by the 2D potential well but finally expand out of the laser focus spot and get lost.

hollow symbols in Fig. 7. The size of the laser focus spot in its propagation direction is characterized by twice the Rayleigh length of $2l_R = 2\pi\omega^2/\lambda$ and is calculated to be ∼9.44 mm with $\omega = 40\,\mu$m and $\lambda = 1064$ nm used for the simulation.

Figure 8 shows the spatial distribution of the decelerated molecular packet in the planes of (a) XY, (b) XZ, and (c) YZ of the laboratory frame when the velocity of the hybrid potential well is decelerated to 50 m/s at the angle of $\theta = \sim 14.12^\circ$. As one can see, the spatial distribution of the decelerated molecular packet is well confined within the scale of the hybrid potential well, as shown in Fig. 3. The velocity distribution of the decelerated molecular packet in the laboratory frame of XYZ is also examined and corresponding results are shown in Fig. 9.

When the molecular packet is decelerated to the desired longitudinal velocity in the 3D hybrid potential well, the orbiting speed of the laser focus spot can be maintained constant (i.e., $a = 0\,\text{m/s}^2$) and the molecular packet will orbit in the storage ring along with the moving 3D potential well. In a conventional electrostatic storage ring, due to lack of confinement the molecular packet gradually spreads out in the longitudinal direction and finally fills the whole area. Tedious efforts have been made to avoid the spreading of the orbiting molecular packet and to increase the number of its round trips over the years [23,25,32]. For our scheme here, the molecular packet is simply confined in the orbiting 3D potential well with no spreading in the storage ring. Figure 10(a) shows the simulated time-of-flight (TOF) profiles of the orbiting molecular packet with a forward speed of 50 m/s at a selected point of observation in the storage ring. As shown in the figure, the orbiting molecular packet reappears at the selected observation point without spreading in the storage ring. The time interval between neighboring peaks is ∼31.4 ms, corresponding to the round trip time of the orbiting molecular packet in the storage ring. For comparison, the trajectories of the same orbiting molecular packet with absence of the laser field are also simulated, and Fig. 10(b) presents the corresponding TOF profiles of the molecular packet. As one can see, due to lack of confinement the molecular packet gradually gets broader in the storage ring and the height of the TOF profile peaks decreases dramatically. After about seven round trips the molecular packet fills the whole area of the storage ring and is no longer discernible.

IV. ANALYSIS AND DISCUSSION

For efficient deceleration of the molecular beam from supersonic expansion using our scheme, a linear deceleration rate a on the order of $\sim 10^5\,\text{m/s}^2$ for the orbiting laser focus

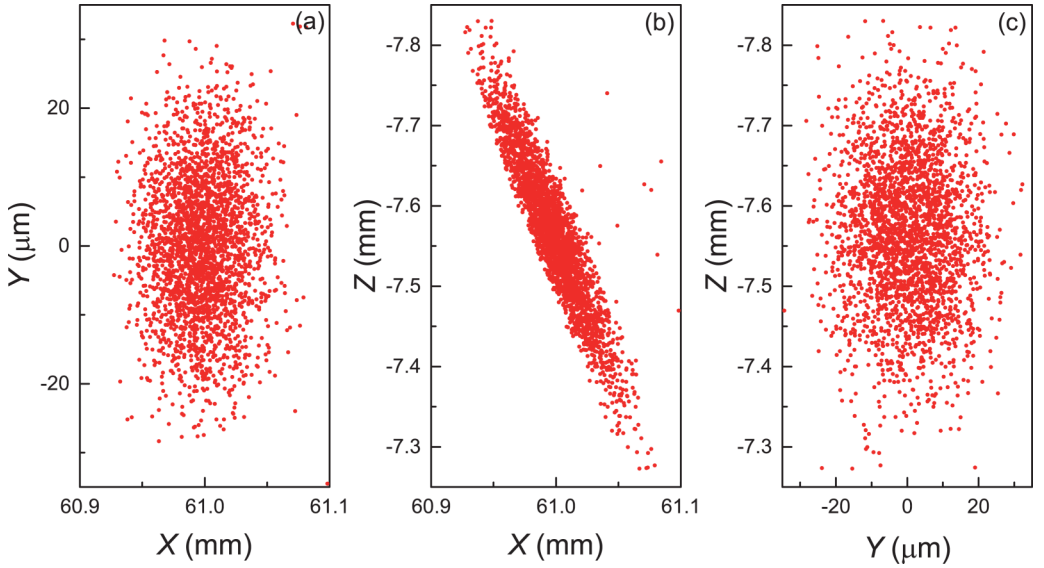

FIG. 8. The spatial distribution of the decelerated molecular packet under hybrid potential well in the planes of (a) XY, (b) XZ, and (c) YZ of the laboratory frame when the velocity of the optical potential well is decelerated to 50 m/s at an angle of $\theta = \sim 14.12^\circ$.

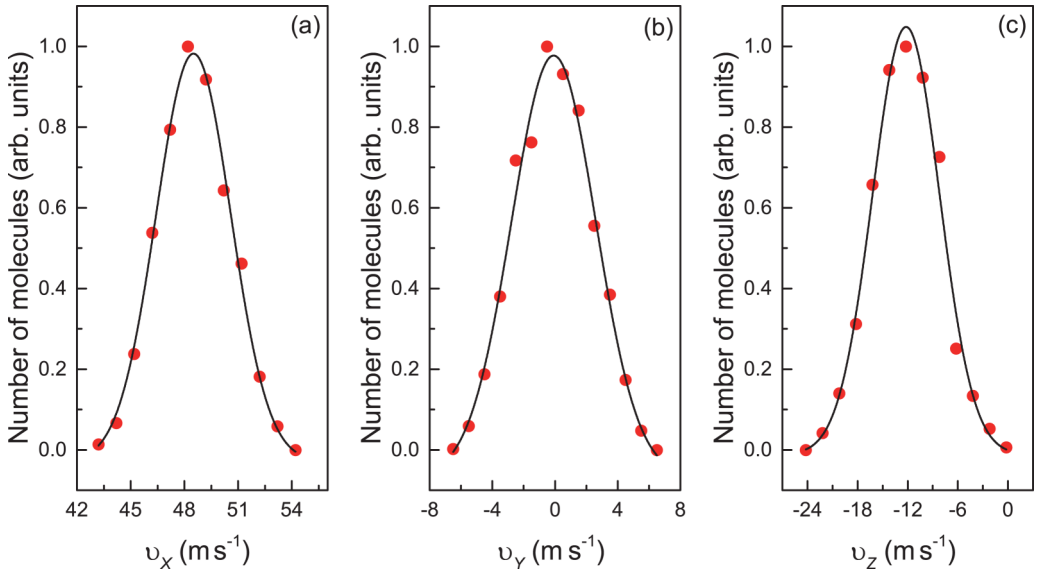

FIG. 9. The velocity distribution of the decelerated molecular packet under hybrid potential well in the planes of (a) XY, (b) XZ, and (c) YZ of the laboratory frame when the velocity of the optical potential well is decelerated to 50 m/s at an angle of $\theta = \sim 14.12^{\circ}$.

spot is essential. This requires an angular deceleration rate γ of the spinning mirror on the order of $10^5 - 10^6$ rad/s^2, which is no longer a challenge for present motor technology [33]. A higher laser power can offer a bigger and deeper potential well for decelerating and trapping more molecules and CW lasers of power up to ~ 500 kW are now commercially available [34]. In fact, the deceleration rate a of the laser focus spot need not be constant during the deceleration process. A stable phase area always exists for the decelerating molecules so long as the value of a does not exceed the maximal force per units mass P_m provided by the potential well. In theory, the smaller the value of a becomes, the larger the area of the phase acceptance will be. Additionally the speed of the decelerated molecular packet is determined by the final speed of the orbiting laser focus spot.

The total number and density of the finally trapped molecules are of decisive significance for their potential application in many fields. The total number can be estimated as $N = \rho V f_1 f_2$. Here ρ is the number density of the molecules. V is the effective volume of the potential trap, which is approximated as $V = \pi w^2 h$ with w the laser beam waist radius and h the effective trap length in the z direction. f_1 is the fraction of molecules in state $|J = 1, \tau = 1, |M| = 1\rangle$; f_2 is the fraction percentage of molecules captured by the potential trap, whose velocities are within the range of $[v - \Delta v, v + \Delta v]$ with v and Δv being the velocity and the velocity acceptance of the trap, respectively. For a laser focus with a waist radius of 40 μm, the effective volume V is $\sim 5 \times 10^{-6}$ cm^{-3}. Suppose that the supersonic H_2O molecular beam loading the potential well has a number density

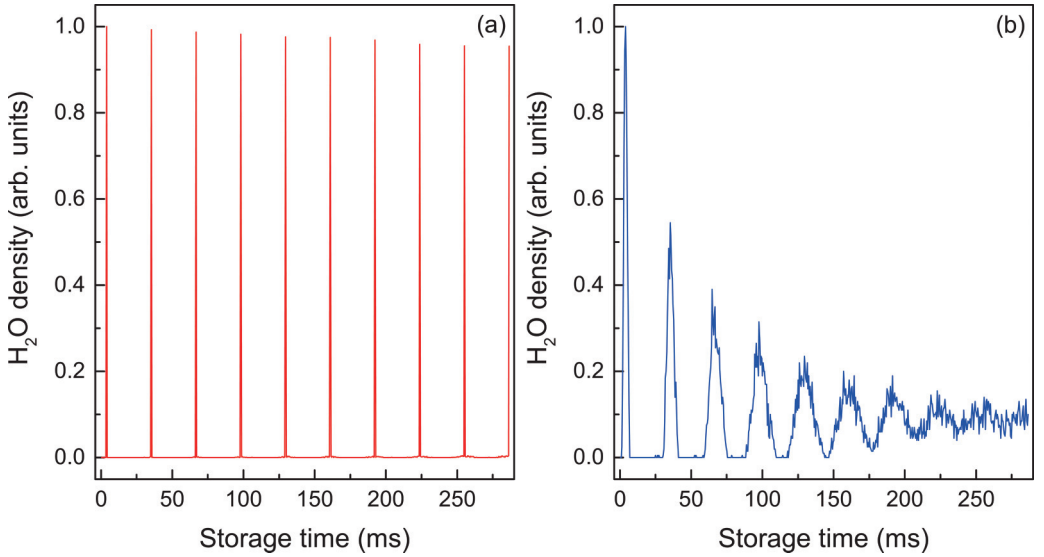

FIG. 10. The simulated time-of-flight (TOF) profiles of the decelerated H_2O molecular packet with the presence (a) and absence (b) of the orbiting laser focus spot of 50 m/s.

of about $10^{13}-10^{14}$ molecules/cm^{-3}. With a translational temperature of $\sim$2 K the fraction f_1 of molecules in state $|J=1,\tau=1,\ |M|=1\rangle$ is about 5%. With a maximal velocity acceptance of about 4.5 m/s (the case of $a=0.5P_m$), the fraction percentage f is then calculated to be $\sim 5\times 10^{-3}$. With all the parameters above, the total number of molecules first captured by the hybrid trap is on the order of 10^4-10^5 with their density being about 10^9-10^{10} molecules/cm^{-3}. These molecular numbers and densities combined with long trap lifetime for molecules are very attractive compared to those from other methods like magneto-optical trapping [9,35] and magnetic trapping [36,37].

V. CONCLUSION

In conclusion, we have theoretically investigated the dynamics of an optoelectrostatic storage ring for polar molecules. The potentials of water molecules experienced in the combined optical and electrical fields are calculated using the matrix method. A 3D hybrid potential well for molecules of interest is formed in the focus spot of the red-detuned laser beam. By changing the spin speed of a reflective mirror, the orbiting speed of the hybrid potential well can be conveniently controlled, which is suitable for manipulation of molecular motion, like deceleration and trapping. The behavior of water molecules inside the decelerating potential well is analyzed in detail, and the Monte Carlo method is used to simulate the deceleration and trapping processes of water molecules from supersonic expansion in the 3D hybrid potential well. Simulation results indicate that water molecules can be well decelerated and trapped in the optoelectrostatic storage ring with high densities.

The scheme proposed here is particularly suitable for decelerating and trapping heavy-atom diatomic molecules like BaF [38], which usually possess a large ratio of polarizability to mass. Heavy polar molecules are very promising candidates for the sensitive electron electric dipole moment (eEDM) measurement, considered as a platform for searching new physics beyond the Standard Model (SM) of elementary physics since the 1950s [39]. Laser cooling of heavy polar molecules is inefficient and usually requires a slowing distance of tens of meters [40]. For our scheme here with the parameters used above, the performed simulation indicates that the BaF molecules of $\sim$250 m/s can be efficiently decelerated to 50 m/s within a distance of about $\sim$5 cm and then trapped in the orbiting 3D potential well of the storage ring. Moreover, the proposed optoelectrostatic storage ring can also serve as an ideal platform for studies like cold collisions and cold chemistry.

ACKNOWLEDGMENTS

This work is supported by the National Natural Science Foundation of China (Grants No. 91536218 and No. 11604100), and the Natural Science Foundation of Shanghai (Grant No. 14ZR1412000).

[1] J. J. Hudson, D. M. Kara, I. J. Smallman, B. E. Sauer, M. R. Tarbutt, and E. A. Hinds, Nature **473**, 493 (2011).
[2] E. R. Hudson, C. Ticknor, B. C. Sawyer, C. A. Taatjes, H. J. Lewandowski, J. R. Bochinski, J. L. Bohn, and J. Ye, Phys. Rev. A **73**, 063404 (2006).
[3] M. A. Baranov, K. Osterloh, and M. Lewenstein, Phys. Rev. Lett. **94**, 070404 (2005).
[4] O. Dutta, M. Jääskeläinen, and P. Meystre, Phys. Rev. A **71**, 051601(R) (2005).
[5] D. DeMille, Phys. Rev. Lett. **88**, 067901 (2002).
[6] A. J. Kerman, J. M. Sage, S. Sainis, T. Bergeman, and D. DeMille, Phys. Rev. Lett. **92**, 153001 (2004).
[7] J. G. Danzl, E. Haller, M. Gustavsson, M. J. Mark, R. Hart, N. Bouloufa, O. Dulieu, H. Ritsch, and H.-C. Nägerl, Science **321**, 1062 (2008).
[8] J. F. Barry, D. J. McCarron, E. B. Norrgard, M. H. Steinecker, and D. DeMille, Nature **512**, 286 (2014).
[9] L. Anderegg, B. L. Augenbraun, E. Chae, B. Hemmerling, N. R. Hutzler, A. Ravi, A. Collopy, J. Ye, W. Ketterle, and J. M. Doyle, Phys. Rev. Lett. **119**, 103201 (2017).
[10] H. L. Bethlem, G. Berden, and G. Meijer, Phys. Rev. Lett. **83**, 1558 (1999).
[11] E. Narevicius, A. Libson, C. G. Parthey, I. Chavez, J. Narevicius, U. Even, and M. G. Raizen, Phys. Rev. Lett. **100**, 093003 (2008).
[12] B. Friedrich, Phys. Rev. A **61**, 025403 (2000).
[13] R. Fulton, A. I. Bishop, and P. F. Barker, Phys. Rev. Lett. **93**, 243004 (2004).
[14] R. Fulton, A. I. Bishop, M. N. Shneider, and P. F. Barker, Nat. Phys. **2**, 465 (2006).
[15] M. S. Elioff, J. J. Valentini, and D. W. Chandler, Science **302**, 1940 (2003).
[16] A. Trottier, D. Carty, and E. Wrede, Mol. Phys. **109**, 725 (2011).
[17] N. R. Hutzler, H.-I. Lu, and J. M. Doyle, Chem. Rev. **112**, 4803 (2012).
[18] M. Zeppenfeld, M. Motsch, P. W. H. Pinkse, and G. Rempe, Phys. Rev. A **80**, 041401(R) (2009).
[19] S. Y. T. van de Meerakker, P. H. M. Smeets, N. Vanhaecke, R. T. Jongma, and G. Meijer, Phys. Rev. Lett. **94**, 023004 (2005).
[20] D. P. Katz, J. Chem. Phys. **107**, 8491 (1997).
[21] F. M. H. Crompvoets, H. L. Bethlem, R. T. Jongma, and G. Meijer, Nature **411**, 174 (2001).
[22] H. Nishimura, G. Lambertson, J. G. Kalnins, and H. Gould, Eur. Phys. J. D **31**, 359 (2004).
[23] C. E. Heiner, D. Carty, G. Meijer, and H. L. Bethlem, Nat. Phys. **3**, 115 (2007).
[24] L. Deng, Y. Xia, and J. Yin, J. Opt. Soc. Am. B **27**, A88 (2010).
[25] S. Hou, B. Wei, L. Deng, and J. Yin, Sci. Rep. **6**, 32663 (2016).
[26] H. L. Bethlem, F. M. H. Crompvoets, R. T. Jongma, S. Y. T. van de Meerakker, and G. Meijer, Phys. Rev. A **65**, 053416 (2002).
[27] L. Deng, S. Hou, and J. Yin, Phys. Rev. A **95**, 033409 (2017).
[28] Y. Yang, S. Hou, and L. Deng, Chin. Phys. B **27**, 053701 (2018).
[29] R. Knacke, H. Larson, and K. S. Noll, Astrophys. J. **335**, L27 (1988).
[30] F. C. DeLucia, P. Helminger, and W. H. Kirchhoff, J. Phys. Chem. Ref. Data **3**, 211 (1974).

[31] T. D. Hain, R. M. Moision, and T. J. Curtiss, J. Chem. Phys. **111**, 6797 (1999).
[32] P. C. Zieger, S. Y. T. van de Meerakker, C. E. Heiner, H. L. Bethlem, A. J. A. van Roij, and G. Meijer, Phys. Rev. Lett. **105**, 173001 (2010).
[33] http://www.maxonmotor.com.au/maxon/view/category/.
[34] http://www.ipgphotonics.com/group/view/8/Lasers%2FHigh_Power_CW_Fiber_Lasers.
[35] S. Truppe, H. J. Williams, M. Hambach, L. Caldwell, N. J. Fitch, E. A. Hinds, B. E. Sauer, and M. R. Tarbutt, Nat. Phys. **13**, 1173 (2017).
[36] D. J. McCarron, M. H. Steinecker, Y. Zhu, and D. DeMille, Phys. Rev. Lett. **121**, 013202 (2018).
[37] H. J. Williams, L. Caldwell, N. J. Fitch, S. Truppe, J. Rodewald, E. A. Hinds, B. E. Sauer, and M. R. Tarbutt, Phys. Rev. Lett. **120**, 163201 (2018).
[38] S. L. Davis, J. Chem. Phys. **89**, 1656 (1988).
[39] E. M. Purcell and N. F. Ramsey, Phys. Rev. **78**, 807 (1950).
[40] J. Lim, J. R. Almond, M. A. Trigatzis, J. A. Devlin, N. J. Fitch, B. E. Sauer, M. R. Tarbutt, and E. A. Hinds, Phys. Rev. Lett. **120**, 123201 (2018).